CONCRETE LIBRARY OF JSCE NO. 38, DECEMBER 2001

AN EXPERIMENTAL STUDY ON SEISMIC RETROFITTING METHODS FOR EXISTING REINFORCED CONCRETE COLUMNS WITH EXTERNAL LATERAL REINFORCEMENT ANCHORED AT FOUR CORNERS OF COLUMNS

(Translation from Proceedings of JSCE, No.662／V－49, November 2000)

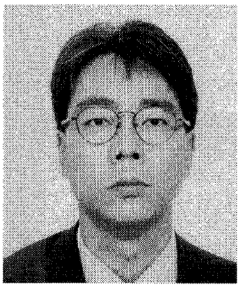
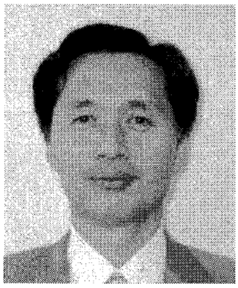
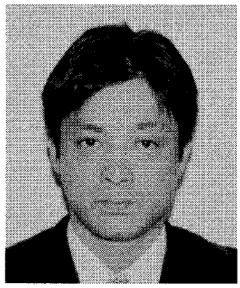
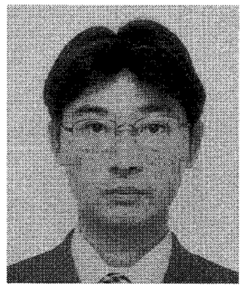

Takeshi TSUYOSHI Tadayoshi ISHIBASHI Masashi KOBAYASHI Shinichi TATSUKI

Since Hyogo-Ken Nanbu Earthquake in 1995, seismic retrofitting of existing RC columns has been carried out. Steel jacket methods are the most commonly adopted, but these methods are not available in the case of RC viaducts whose columns are in contact with or used by shops, store, and houses. Therefore, we have developed a new seismic retrofitting method which can be easily applied in these cases. External lateral reinforcement is arranged around an existing RC column and anchored at the four corners of the column with L-shaped steels. We have carried out cyclic loading tests of columns retrofitted with this method, and confirmed that ductility is much improved.

Key Words : *seismic retrofitting method, reverse cyclic loading, reinforced concrete column, ductility*

Takeshi Tsuyoshi is a group leader in the Tokaido Sobu Department at the Tokyo Construction Office of East Japan Railway Company. He obtained his D.Eng from Tokyo University in 2001. His research interests relate to the seismic design of concrete structures for railways. He is a member of the JSCE.

Tadayoshi Ishibashi is a manager in the Structural Engineering Center of the Construction Department of East Japan Railway Company. He obtained his D.Eng from Tokyo University in 1983. His research interests relate to the seismic design of concrete structures for railways. He is a fellow of the JSCE.

Masashi Kobayashi is a senior chief engineer at the Oyama Construction Depot of the Joshinetsu Construction Office of East Japan Railway Company. His research interests relate to the seismic design of concrete structures for railways. He is a member of the JSCE.

Shinichi Tatsuki is an engineer in the Construction Management Department of the Tohoku Construction Office of East Japan Railway Company. His research interests relate to the seismic design of concrete structures for railways. He is a member of the JSCE.

1. Introduction

After the Hanshin-Awaji Earthquake Disaster of Jan.17, 1995, the authorities at the Ministry of Transportation issued a notification on seismic retrofitting to railway companies. Following the recommendations of this notification, seismic retrofitting of the columns of reinforced concrete rigid-frame structures that have a shear-to-moment capacity ratio of below 1.0 has been carried out. Steel jacket methods have been adopted in general for this purpose. Within the service area of the East Japan Railway Company, about ten thousand columns have been retrofitted at present on the Shinkannsen Lines and conventional lines in Minami-Kanto and Sendai Areas.

The space under railway viaducts is often used in some way by stores and offices, especially in urban areas. This can make it very difficult for large construction machinery like cranes, which are used for steel jacket methods, to gain access to sites. In such cases, steel jacket methods entail a large amount of extra work to remove obstacles as well as payments to stores or offices. In these cases, seismic retrofitting is rarely carried out.

We have developed a new seismic retrofitting method to overcome this limitation in which external lateral reinforcement is arranged around an existing RC column and anchored at the four corners with L-shaped steels. The materials used for this method are steel bars, L-shaped steel anchorages, and mortar for anchorages, all of which are small items. As a result, this method can be executed by hand only and is easily applied to existing RC columns in confined spaces. In this research, we carried out reverse cyclic loading tests of RC columns retrofitted using our proposed method. The effects of seismic retrofitting were examined through experimental results of half-size specimens simulating columns on actual railway structures.

2. Experimental Procedure

2.1 Specimens

Table 1 shows the properties of all the specimens and the strengths of the materials used. Figure 1 shows the vertical and horizontal sections of all specimens. Figure 2 shows the anchorages for the external lateral reinforcement in detail. These anchorages consist of L-shaped steel and mortar. Threaded reinforcing bars are used and these are anchored with lock nuts. Lock nuts are tightened by a hand wrench.

Standard specimens have a section of 400 mm x 400 mm, which is half that of the actual columns. The ratio of shear span to effective depth is 3.19 in most specimens, and the axial compressive stress is basically 0.98 N/mm^2. The axial reinforcement ratio was determined by considering that the actual reinforcement ratio of existing RC columns is about 3% and that the ratio of shear capacity to flexural capacity of the standard specimen I should be less than 1.0.

Table 2 shows calculated characteristic values for the specimens. P_{ycal} is the calculated horizontal force when the axial reinforcement at the bottom of the columns, which is nearest to compressive end, reaches yield. P_{ucal} is the calculated horizontal force when the sectional force at the bottom reaches the ultimate flexural strength. V_{yd} is the calculated value of ultimate shear strength of the section, and V_{mu} is equal to P_{ucal}. The ultimate strength is calculated based on actual material strength [1]. In calculating the shear strength, the shear force held by external lateral reinforcement is estimated by truss theory using the following equations:

$$V_{yd}=V_c+V_s \qquad (1)$$

$$V_c=f_{vc}\cdot(f'_c)^{1/3}\cdot\beta_d\cdot\beta_p\cdot\beta_n\cdot b_w\cdot d \qquad (2)$$

$$V_s=A_w\cdot f_{wyd}/s_s\cdot z \qquad (3)$$

where,
V_{yd}: ultimate shear strength (kN),
V_c: ultimate shear strength without shear reinforcement (kN),
V_s: ultimate shear strength held by shear reinforcement (kN),

$f_{vc}=0.20(0.75+1.4\cdot d/a)$

$\beta_d=(1000/d)^{1/4}\leqq 1.5$

$\beta_p=(100p_c)^{1/3}\leqq 1.5$

$\beta_n=1+2M_0/M_u\leqq 2$

b_w: width of section (mm),
d: effective depth of section (mm),
p_c: axial reinforcement ratio,

$p_c=A_s/(b_w \cdot d)$

A_s: area of axial reinforcement in the section [2],
M_u: ultimate flexural strength,
M_o: decompression moment,
f'_c: compressive strength of concrete (N/mm^2),
A_w: area of external lateral reinforcement in the section s_s (mm^2),
f_{wyd}: yield strength of lateral external reinforcement (N/mm^2),
s_s: spacing of lateral external reinforcement (mm),
z=d/1.15

Standard specimen I has no lateral reinforcements. Specimens II-VII are retrofitted specimens. All retrofitted specimens contain no ordinary hoop reinforcements inside the section. The ratio of shear capacity to flexural capacity (V_{yd}/V_{mu}) of specimen II is 2.35. In this specimen, the external lateral reinforcement touches the surface of the column and the reinforcing bar is covered with post-cast mortar.

In the III series of specimens, post-cast mortar is used only at anchorages, and the lateral reinforcement itself is exposed. V_{yd}/V_{mu} is set from 1.06 to 2.38 by changing the external lateral reinforcement ratio, and the lateral reinforcement touches the surface of the column. Specimens III-1 and III-2 have anchorages of Type A, while III-3 has anchorages of Type C. Type A and C anchorages have the same anchoring characteristics because they have the same bearing area.

In the IV series of specimens, post-cast mortar is used only at anchorages, and the lateral reinforcement is exposed. V_{yd}/V_{mu} is set from 0.93 to 1.41 by changing the external lateral reinforcement ratio. The separation between external lateral reinforcement and the surface of the column is 20 mm. This is because in actual retrofitting executions, lateral reinforcement cannot always be arranged flush against the surface of the column because the surface of the column is not always flat. The IV series of specimens have larger L-shaped steel than the III series in order to secure the 20 mm separation. However, the bearing areas of the anchorages are same in both series.

In the V series of specimens, anchorages are separated at each rung of the external lateral reinforcement in the axial direction. In specimen V-1, the anchorages are separated but are in contact with each other in the axial direction. V_{yd}/V_{mu} is 2.38, and the lateral reinforcement touches the surface of the column in specimen V-1. Specimens V-2, V-3, and V-4 have a lower lateral reinforcement ratio than specimens V-1, and their V_{yd}/V_{mu} is about 1.5. Their anchorages are separated in the axial direction. The separation between external reinforcement and the surface of the column is 20 mm in specimen V-2, and 25 mm in specimen V-3 and V-4.

Next, in the VI series of specimens, the size of the section is 600 mm x 600 mm. The anchorages are unified in the axial direction, and the lateral reinforcement touches the surface of the column. Their V_{yd}/V_{mu} ratios are 1.52 and 2.27.

Finally, in the VII series of specimens, the axial compressive stress is set as +5.89 (N/mm^2) and 9.81 (N/mm^2), and their V_{yd}/V_{mu} is about 1.5. This series models the case of central columns of large underground structures. Specimen VII-2 has a section of 300 mm x 300 mm, and the separation between lateral reinforcement and the surface of the column is 15 mm.

Table 3 lists the experimental parameters described above.

As shown in Figure 1, some space is secured between the lower edge of the anchorages and the footings in order to ensure that the anchorages do not affect ultimate flexural strength.

Table 1 Properties of all specimens and strength of materials used

Specimen number	Section (mm×mm)	Effective depth (mm)	Shear span a (mm)	a/d	Arrangement of axial reinforcement (number)	Ratio of axial reinforcement $A_s/(b \cdot d)$ (%)	Arrangement of lateral external reinforcement (mm)	Ratio of lateral external reinforcement $A_w/(b \cdot s)$ (%)	Axial compressive stress (N/mm²)	Material strength: Column concrete (N/mm²)	Footing concrete (N/mm²)	Anchorage mortar (N/mm²)	Yield strength of axial reinforcement (N/mm²)	Yield strength of lateral reinforcements (N/mm²)	Yield strain of axial reinforcement	Yield strain of lateral reinforcement	Details of anchorage: Shape of anchorage	L1 (mm)	L2 (mm)
I	400×400	360	1150	3.19	D19×16	3.18	—	—	0.98	23.2	23.2	—	370.5	—	2031	—	—	—	—
II	400×400	360	1150	3.19	D19×16	3.18	D13@65	0.98	0.98	26.6	26.5	45.3	377.2	354.6	2072	1931	TypeA	—	25
III−1	400×400	360	1150	3.19	D19×16	3.18	D13@65	0.98	0.98	20.1	20.7	47.6	377.2	354.6	2072	1931	TypeA	40	25
III−2	400×400	360	1150	3.19	D19×16	3.18	D13@150	0.42	0.98	35.7	35.7	61.9	382.8	371.7	2092	2018	TypeA	40	25
III−3	400×400	360	1150	3.19	D19×20	3.98	D13@200	0.32	0.98	32.5	32.5	25.8	382.8	371.7	2092	2018	TypeC	40	—
IV−1	400×400	360	1150	3.19	D19×16	3.18	D13@150	0.42	0.98	32.5	32.5	55.5	382.8	371.7	2092	2018	TypeB	40	—
IV−2	400×400	360	1150	3.19	D19×20	3.98	D13@200	0.32	0.98	31.8	31.8	45.3	382.8	371.7	2092	2018	TypeB	40	—
V−1	400×400	360	1150	3.19	D19×16	3.18	D13@65	0.98	0.98	32.9	32.9	50.0	382.8	371.7	2092	2018	TypeA	40	25
V−2	400×400	360	1150	3.19	D19×16	3.18	D13@150	0.42	0.98	33.6	33.6	46.9	378.5	395.7	1981	2012	TypeB	40	—
V−3	400×400	360	1150	3.19	D19×16	3.18	D13@150	0.42	0.98	43.2	43.2	40.5	378.5	395.7	1981	2012	TypeD	40	—
V−4	400×400	360	1150	3.19	D19×16	3.18	D13@150	0.42	0.98	39.4	39.4	40.5	378.5	395.7	1981	2012	TypeD	40	—
VI−1	600×600	550	1650	3.00	D25×24	3.69	D22@200	0.65	0.98	27.6	27.6	51.3	368.0	368.2	2006	1981	TypeC	60	—
VI−2	600×600	550	1650	3.00	D25×24	3.69	D29@200	1.07	0.98	33.0	33.0	53.9	368.0	391.9	2006	2108	TypeC	60	—
VII−1	400×400	360	1150	3.19	D19×16	3.18	D13@125	0.51	5.89	36.5	32.5	60.3	368.7	356.2	2051	2116	TypeB	40	—
VII−2	300×300	260	950	3.65	D16×16	4.07	D13@150	0.56	9.81	35.3	35.9	62.6	358.1	356.2	1995	2116	TypeB	40	—

Table 2 Calculated values and testing values

Specimen number	Calculated values: P_{ycal} (kN)	P_{ucal} (kN)	V_c (kN)	V_s (kN)	V_c/V_{mu}	V_s/V_{mu}	V_{yd}/V_{mu}	δ_{y1} (mm)	δ_{y0} (mm)	δ_{ycal} (mm)	Experimental values: P_{ytest} (kN)	P_{utest} (kN)	δ_{yexp} (mm)	δ_{uexp} (mm)	ductility ratio μ
I	196.3	247.0	159.9	0.0	0.65	0.00	0.65					210.0			
II	201.7	255.1	166.8	432.7	0.65	1.70	2.35	1.94	3.96	5.90	234.3	305.9	5.2	97.4	17.7
III−1	197.3	245.9	153.0	432.7	0.62	1.76	2.38	2.41	4.17	6.58	220.6	288.4	5.2	87.6	13.3
III−2	209.3	268.2	183.4	196.5	0.68	0.73	1.42	1.54	3.79	5.33	225.4	305.1	5.1	85.5	16.0
III−3	249.3	317.2	190.3	147.4	0.60	0.46	1.06	1.86	4.01	5.87	290.5	363.0	5.6	76.1	13.0
IV−1	207.7	265.4	178.5	196.5	0.67	0.74	1.41	1.66	3.85	5.51	210.8	295.3	5.5	80.9	14.7
IV−2	248.8	316.4	147.4	147.4	0.47	0.47	0.93	1.89	4.03	5.92	286.7	344.3	6.7	77.8	13.1
V−1	208.0	265.8	178.5	453.5	0.67	1.71	2.38	1.65	3.85	5.50	236.4	310.0	5.3	102.4	18.6
V−2	206.3	264.2	180.5	209.2	0.68	0.79	1.48	1.47	3.65	5.12	228.6	274.7	5.9	66.6	13.0
V−3	210.5	270.3	196.2	209.2	0.73	0.77	1.50	1.19	3.48	4.67	226.4	298.2	5.0	80.2	17.2
V−4	209.0	268.8	190.3	209.2	0.71	0.78	1.49	1.28	3.54	4.82	230.4	292.3	5.0	62.7	13.0
VI−1	541.9	690.6	370.8	681.7	0.54	0.99	1.52	2.40	4.49	6.89	570.9	777.9	7.9	102.9	14.9
VI−2	549.2	705.5	393.4	1204.7	0.56	1.71	2.27	2.07	4.37	6.44	541.3	769.1	8.0	101.4	15.7
VII−1	282.2	331.7	224.6	226.0	0.68	0.68	1.36	1.90	3.96	5.86	334.7	392.4	4.9	62.9	10.8
VII−2	178.8	192.3	151.1	136.0	0.79	0.71	1.49	2.11	4.22	6.33	223.3	248.2	4.6	49.3	7.8

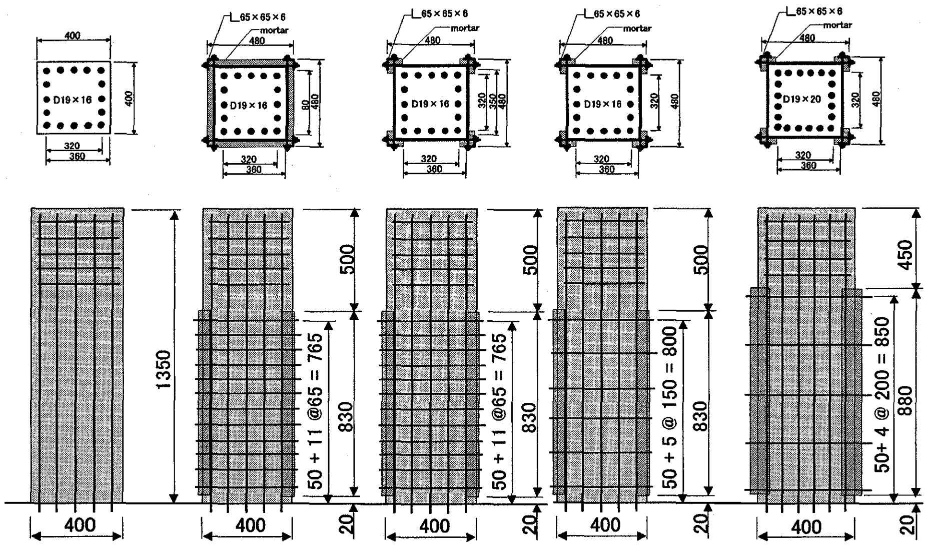

(a)I (b)II (c)III-1 (d)III-2 (e)III-3

Figure 1 Vertical and horizontal sections

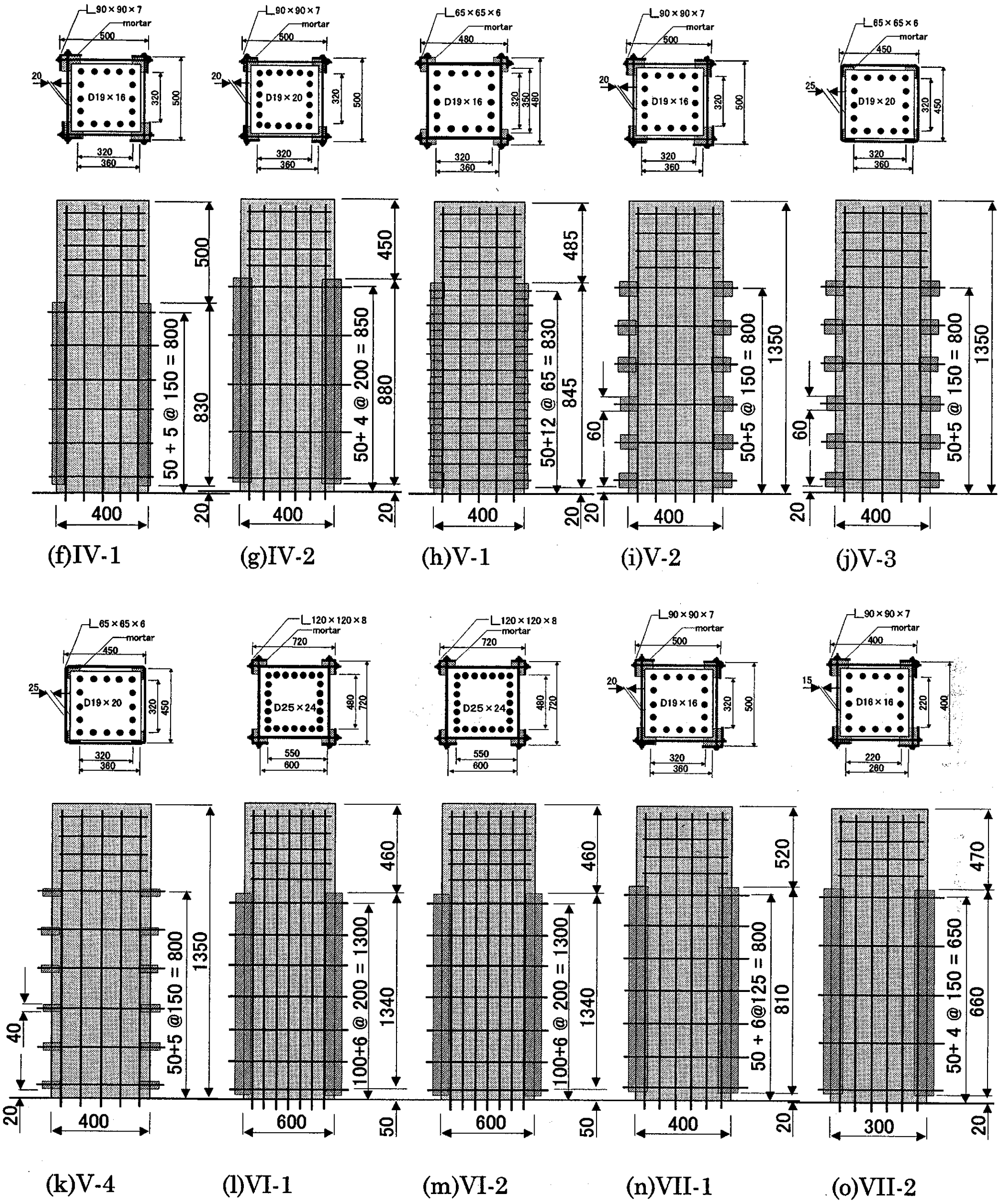

Figure 1 Vertical and horizontal sections

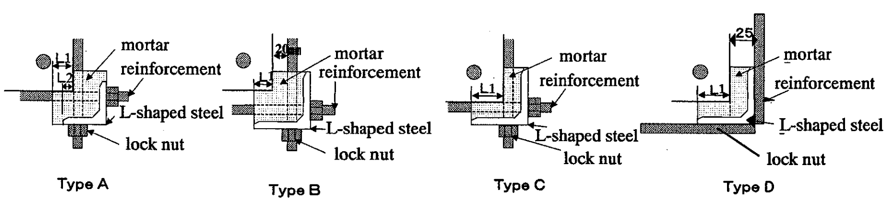

Figure 2 Anchorages in detail

Table 3 List of experimental parameters

Specimen number	Additional cover mortar	V_{yd}/V_{mu}	Separation between column surface and lateral reinforcement (mm)	Separation of L-shaped steel	Section size (mm)	Compressive axial stress (N/mm^2)
I	—	0.65	0	—	400×400	0.98
II	exist	2.35	0	no	400×400	0.98
III−1	no	2.38	0	no	400×400	0.98
III−2	no	1.42	0	no	400×400	0.98
III−3	no	1.06	0	no	400×400	0.98
IV−1	no	1.41	20	no	400×400	0.98
IV−2	no	0.93	20	no	400×400	0.98
V−1	no	2.38	0	exist	400×400	0.98
V−2	no	1.48	20	exist	400×400	0.98
V−3	no	1.5	25	exist	400×400	0.98
V−4	no	1.49	25	exist	400×400	0.98
VI−1	no	1.52	0	no	600×600	0.98
VI−2	no	2.27	0	no	600×600	0.98
VII−1	no	1.36	20	no	400×400	5.89
VII−2	no	1.49	15	no	300×300	9.81

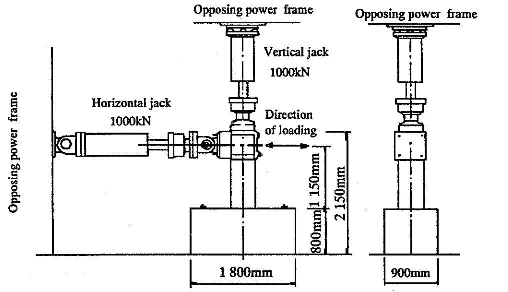

Shear span is 1,650mm for VI-1,2 and 950 mm for VII-2.
Height of footing is 700 mm for VI-1,2 and 800 mm for VII-2

Figure 3 Loading systems

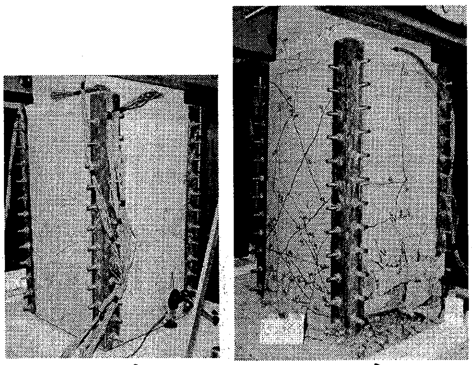

(a)after 1 δ_{ytest} (b)after 14 δ_{ytest}

Picture 1 Specimen II

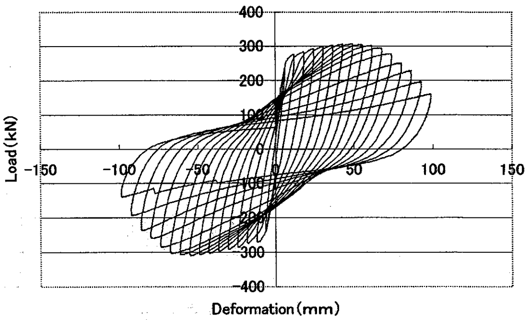

Figure 4 Cyclic load-displacement relation of II

2.2 Loading systems

Figure 3 shows the loading systems. All specimens were tested under constant axial load, and reverse static cyclic displacement was applied. The standard yield deformation of each specimen (δ_{ytest}) is defined as the experimental deformation at which the reinforcement which has the largest effective depth reaches yield. Loading was carried out up to δ_{ytest} under load control with a loading step of 4.9 - 9.8 kN. Thereafter, cyclic displacement at an integer number multiple of δ_{ytest} was applied ($2\delta_{ytest}$, $3\delta_{ytest}$, $4\delta_{ytest}$, $\cdots$). At each loading displacement, one cycle was applied. The period of each loading cycle was at least 120 seconds. The loading test was continued until the horizontal force fell to less than 50 % of the ultimate horizontal strength.

3. Experimental Results and Discussion

3.1Damage to columns

Picture 1 shows the damage to specimen II at the yield point and at the ultimate point (ultimate point: point where horizontal force falls below yield load). Figure 4 shows the cyclic load-displacement relation for specimen II. In the case of this specimen, the number of bending and shear cracks on the surface of the post-cast mortar was less than on the general RC specimen at the yield point. Beyond the yield point, bending and shear cracks increased and the horizontal force gradually became larger. Bending and shear cracks were notable in the range of 1 D (D: effective depth of the section) from the footing. This specimen failed in flexure with crushing of the concrete at the compressive end and buckling of the axial reinforcement.

Pictures 2 to 4 show damage to specimens III-1 to III-3 at the yield point, the ultimate point, and after loading tests. Figure 5 shows the cyclic load-displacement relation of III-1. In case of the III series of specimens, cracking was similar to that of a general RC specimen at the yield point. Until the maximum load point from the yield point, bending and shear cracks become notable in the range of 1 D from the footing. Thereafter, in the case of specimens III-1 and III-2, flexural failure occurred with spalling of the cover concrete and buckling of the axial reinforcement in the range of 1 D from the footing. In case of III-3, which had a slightly smaller ratio of external lateral reinforcement than the others in the series, the lateral load gradually decreased as buckling of the axial reinforcement occurred in the range of 1 D from the footing. The failure type of III-3 was shear failure after yielding with a large shear crack.

Pictures 5(a) and (b) show the damage after loading to IV-1 and IV-2. Figure 6 shows the cyclic load-displacement relation for this specimen. One of the characteristics of the IV series is the separation between the external lateral reinforcement and the surface of the column. Compared with the III series, spalling of the cover concrete and buckling of the reinforcement occurred earlier, and both effects were observed in the range of 1.5 D from the footing. Otherwise, failure was almost the same as the III series.

Pictures 5 (c) - 5(f) show the damage after loading to V-1, V-2, V-3, and V-4. Separation of the anchors had little influence on failure conditions when the other parameters such as lateral reinforcement ratio, separation between the surface of the column and external lateral reinforcement were unchanged. However, in the case of V-2 and V-4, the load decreased suddenly with failure of the anchorages. Specimens V-3 and V-4 had a 25 mm separation between the lateral reinforcement and the surface of the column. Though a little larger than in other specimens, this greater separation had little influence on failure conditions.

Pictures 5 (g) and (h) show the damage after loading to IV-1 and IV-2, which had sections larger than other specimens. The size of the section hardly affected the damage, which was almost the same as to III-2.

Pictures 5 (i) and (j) show the damage to VII-1 and VII-2, in which high compressive stress was applied. In these cases also, the load gradually decreased as the axial reinforcement started buckling and the cover concrete began spalling in the range of 1D from the footing. However, the load ultimately dropped suddenly in contrast with the s pecimens with less compressive stress.

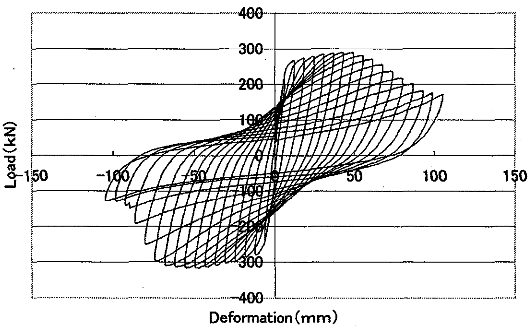

Figure 5 Cyclic load-displacement relation of III-1

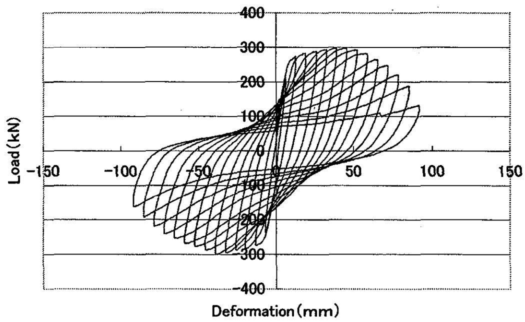

Figure 6 Cyclic load-displacement relation of IV-1

3.2Effects of retrofitting and influence of each parameter

a) Effects of new retrofitting method

Figure 7 shows the envelopes of cyclic load-displacement relations of specimens I, II, and III-1. Specimen I has no lateral reinforcement. The section of specimen II is all covered with post-cast mortar. The section of III-1 is covered only at anchorages with post-cast mortar. The ratio of shear capacity to flexural capacity of II and III-1 is 2.5. As can be seen in Figure 7, deformability was increased as a result of these retrofitting methods. Post-cast mortar had little influence on the deformability of the columns.

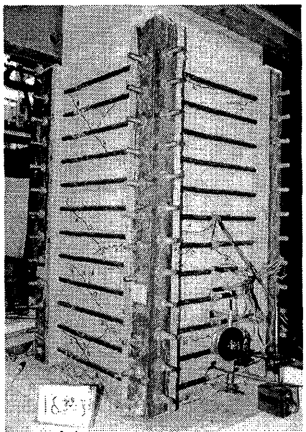

(a) after $1\delta_{ytest}$

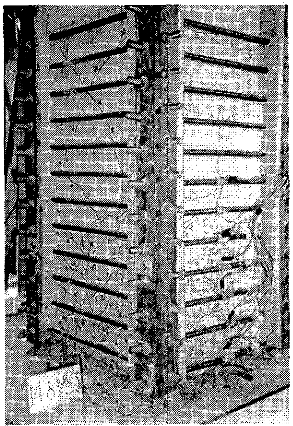

(b) after $14\delta_{ytest}$

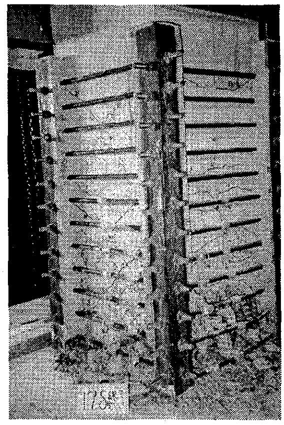

(c) after test

Picture 2 Specimen Ⅲ－1

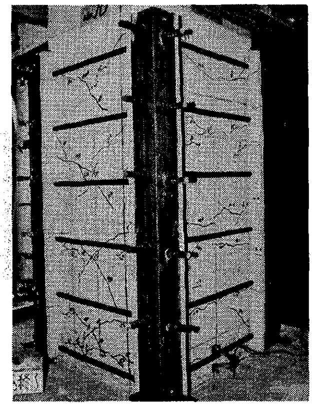

(a) after $1\delta_{ytest}$

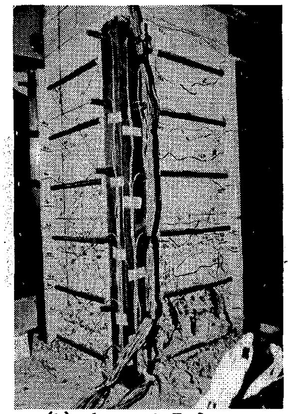

(b) after $15\delta_{ytest}$

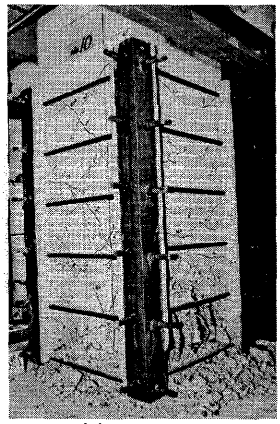

(c) after test

Picture 3 Specimen Ⅲ－2

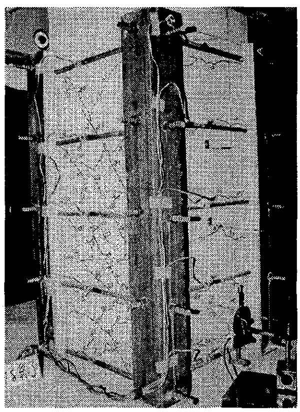

(a) after $1\delta_{ytest}$

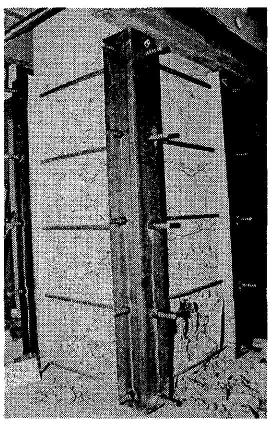

(b) after $9\delta_{ytest}$

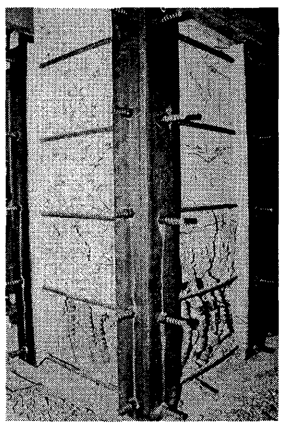

(c) after test

Picture 4 Specimen Ⅲ－3

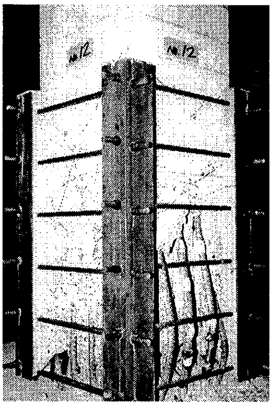

(a) Ⅳ—1

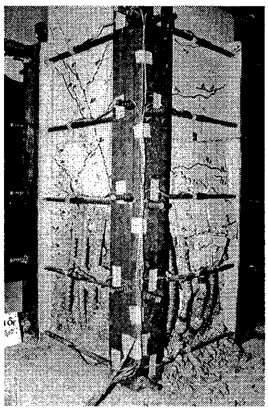

(b) Ⅳ—2

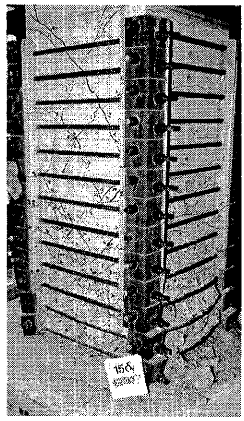

(c) Ⅴ—1

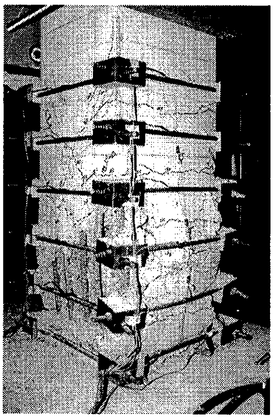

(d) Ⅴ—2

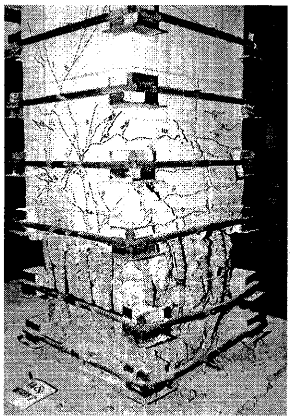

(e) Ⅴ—3

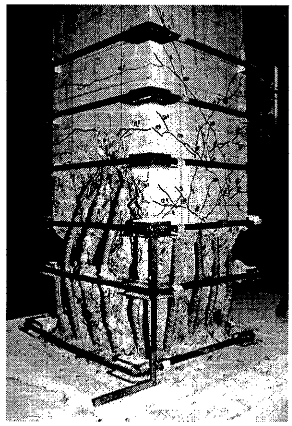

(f) Ⅴ—4

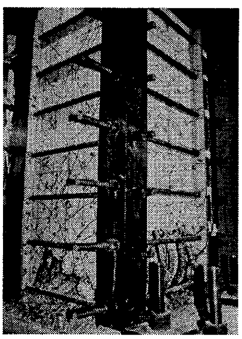

(g) Ⅵ—1

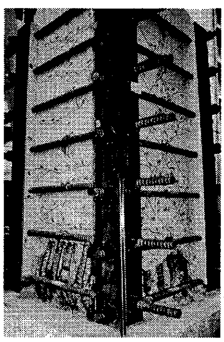

(h) Ⅵ－2

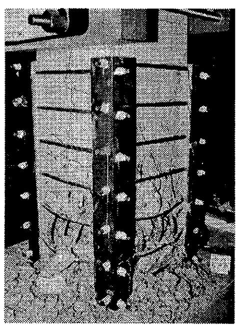

(i) Ⅶ—1

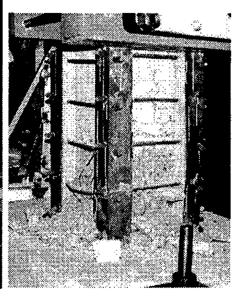

(j) Ⅶ—2

Picture 5 Damage condition after tests

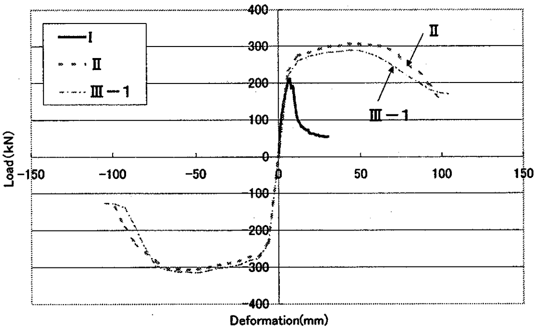

Figure 7 Envelope of cyclic load-displacement relations for specimens I, II, and III-1

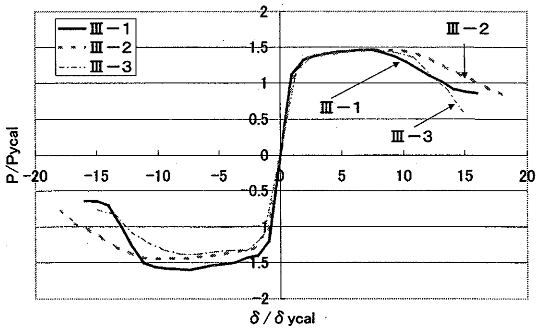

Figure 8 Envelope of cyclic load-displacement relations for specimens III-1, III-2, and III-3

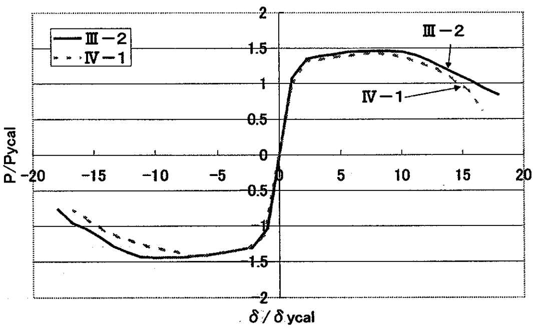

Figure 9 Envelope of cyclic load-displacement relations for specimens III-2 and IV-1

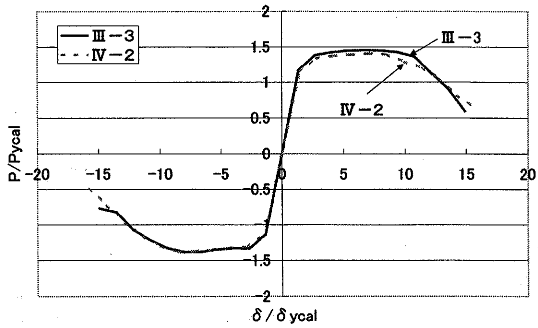

Figure 10 Envelope of cyclic load-displacement relations for specimens III-3 and IV-2

b) Ratio of shear capacity to flexural capacity
Fi gure 8 shows the envelopes of cyclic load-displacement relations for III-1, III-2, and III-3. The ratio of shear capacity to flexural capacity of III-1 is 2.38, 1.42 in the case of III-2, and 1.06 in the case of III-3. The x-axis is a non-dimensional value obtained by dividing displacement by the yield displacement, and the y-axis is a non-dimensional value consisting of the horizontal force divided by the yield force. Specimen III-2, whose shear-to-flexural capacity ratio is 1.42, had the largest ductility. Specimens III-1 and III-3 had almost the same ductility. Th ese experiments confirm that ductility is almost constant if the shear-to-flexural capacity ratio is over 1.0. However, the failure suffered by III-3 was shear failure.

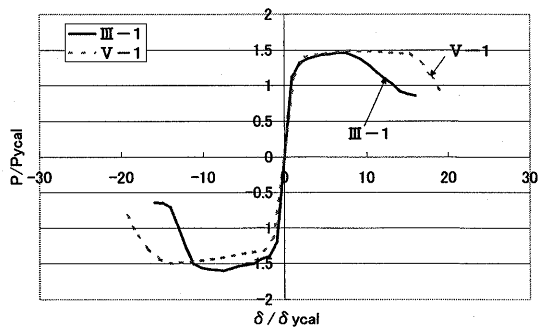

Figure 11 Envelope of cyclic load-displacement relations for specimens III-1 and V-1

c) Separation between external lateral reinforcement and surface of column
Figure 9 shows the envelopes of cyclic load-displacement relations for III-2 and IV-1, while Figure 10 shows the same relations for III-2 and IV-2. In III series, the external lateral reinforcement was in contact with the column, whereas in the IV series, there is a separation of 20 mm. Figure 9 shows that the ductility of specimen IV-1 with the 20 mm separation is a little less than that of III-2. Figure 10 shows that III-3 and IV-2, whose shear-to-flexural capacity ratios are 1.0, has almost the same ductility. Judging from these results, it can be said that separation between the external lateral reinforcement and the surface of the column has little affect on the ductility of retrofitted columns.

d) Separation of anchor parts
Figure 11 shows the envelopes of cyclic load-displacement relations for Specimens III-1 and V-1. The difference

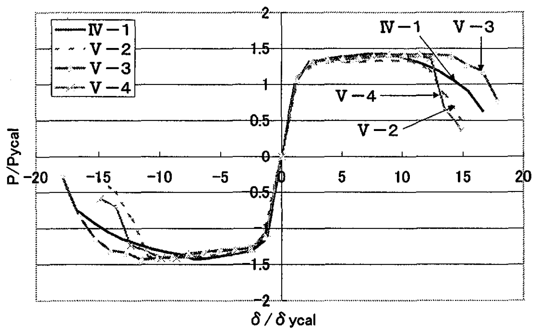

Figure 12 Envelope of cyclic load-displacement relations for specimens IV-1,V-2, V-3, and V-4

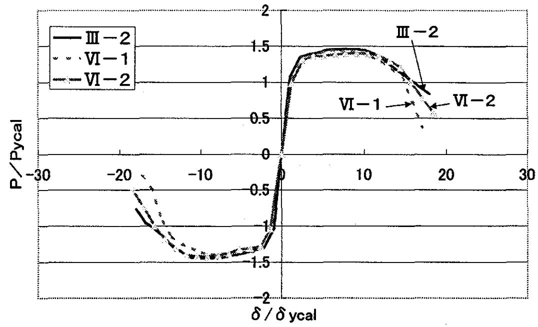

Figure 13 Envelope of cyclic load-displacement relations for specimens III-2,VI-1, and VI-2

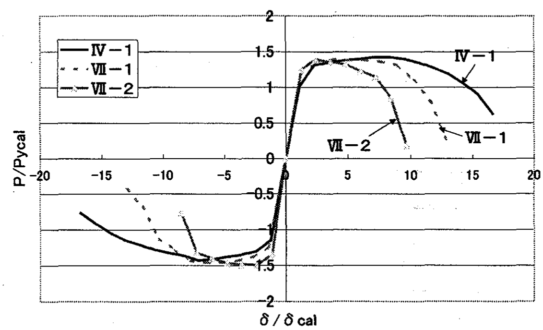

Figure 14 Envelope of cyclic load-displacement relations for specimens IV-1, VII-1, and VII-2

between these two specimens is the continuity of the anchorages in the column axial direction. Other parameters for these specimens are almost the same. As shown in Figure 11, V-1 has greater ductility. Therefore, it can be said that separating the anchorages has some influence on the ductility of the columns. Figure 12 shows the envelopes of cyclic load-displacement relations for specimens IV-1, V-2, V-3, and V-4. In these specimens, the main parameter is the size of shaped steel at the anchorages, while the other parameters are almost constant. In the case of V-2 and V-4, the anchorages were crushed and the load decreased suddenly. On the other hand, in the case of V-3, the anchorages survived and higher ductility was attained. Therefore, in the use of this retrofitting method, adequate ductility is achieved as long as the anchorages remain undamaged.

e) Section size
Figure 13 shows the envelopes of cyclic load-displacement relations for specimen III-2 with a 400 mm square section and specimen VI-1 with a 600 mm square section. Other parameters are almost the same for these specimens. Both specimens exhibited almost the same ductility, as indicated in Figure 13. Specimen VI-1, whose shear-to-flexural capacity ratio is 1.52, and specimen VI-2 (shear-to-flexural capacity ratio = 2.27) had almost the same ductility. Ductility was not increased even if the shear-to-flexural capacity ratio was exceeded 1.5. This tendency was the same in the case of smaller specimens with a 400 mm square section.

f) Axial forces
Figure 14 shows the envelopes of cyclic load-displacement relations for specimen IV-1 with an axial compressive stress of 0.98 (N/mm^2), specimen VII-1 (5.89 (N/mm^2)), and specimen VII-2 (9.91 (N/mm^2)). In the case of higher axial compressive stress, ductility fell with a sudden drop in load.

3.3 Yield displacement

Table 2 shows experimental values of yield load (P_{ytest}), experimental values of maximum load (δ_{yexp}), experimental values of ultimate displacement, and calculated values of yield displacement (δ_{ycal}). Here, the calculated values are obtained using equations (4), (5), (6).

$$\delta_{ycal} = \delta_{y0} + \delta_{y1} \quad (4)$$

$$\delta_{y1} = \Delta l_y \cdot a/(d-x_y) \quad (5)$$

$$\Delta l_y = 7.4\alpha \cdot \varepsilon_y(2+3500\varepsilon_y)\phi/(f'_c)^{2/3} \quad (6)$$

Where,

δ_{ycal}: calculated value of yield displacement,

δ_{y0}: displacement of column member[3],

δ_{y1}: rotational displacement caused by the pullout of axial reinforcement from the footing,

Δl_y: pullout of axial reinforcement from the footing,

x_y: neutral axis at yield,
a: shear span,
d: effective depth of section,

$\alpha = 1+0.9\exp(0.45(1-c_s/\phi))$

ε_y: yield strain of axial reinforcement,

ϕ: diameter of axial reinforcement,

c_s: separation of axial reinforcements

Figure 15 shows the compares the experimental values (δ_{yexp}) and calculated values (δ_{ycal}) of yield displacement. The two correlate well. These experimental values (δ_{yexp}) of yield displacement (δ_{yexp}) are the displacements measured when the test horizontal load reached the calculated value (P_{ycal}). Thus, δ_{yexp} is different from δ_{ytest} defined in the section of 2."OUTLINE OF EXPERIMENTS paragraph" (2) "Loading method".

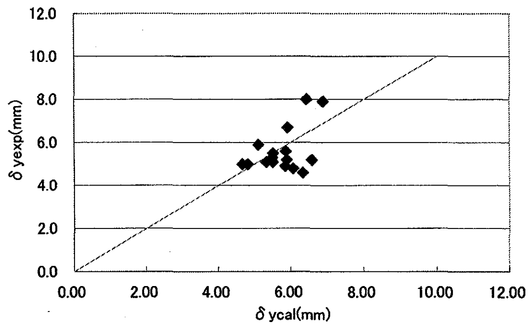

Figure 15 Comparison between experimental values (δ_{yexp}) and calculated values (δ_{ycal}) of yield displacements

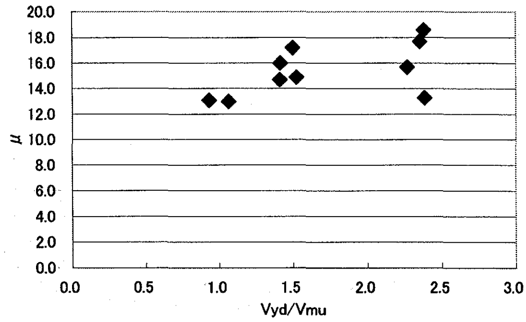

Figure 16 Relationship between V_{yd}/V_{mu} and ductility

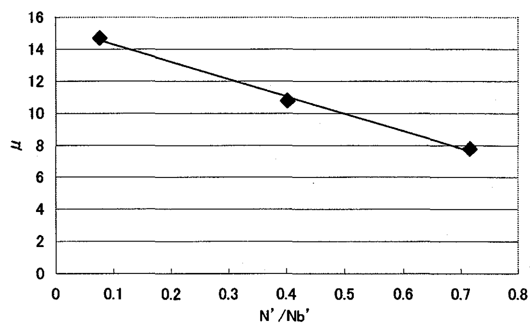

Figure 17 Relations between N'/N_b' and ductility

3.4Ductility ratios

Table 2 shows experimental values of ductility ratio. Ductility ratio is defined as the ratio of experimental ultimate displacement to calculated yield displacement. Here, experimental ultimate displacement is defined as the displacement at which load falls to the yield force. Figure 16 shows the relationship between shear-to-flexural capacity ratio (V_{yd}/V_{mu}) and ductility ratio (μ) when the axial compressive stress is 0.98 N/mm^2. In this figure, specimens V-2 and V-4 are omitted because they failed as a result of damage to the anchorages. As shown in Figure 16, the relationship between shear-to-flexural capacity ratio and ductility ratio indicates a weak, one-dimensional positive correlation. Judging from these experimental results, the ductility ratio rises above over 10 when the shear-to-flexural capacity ratio is over 1.0, and above over 15 for a shear-to-flexural capacity ratio of more than 1.4.

Figure 17 shows the relations between axial compressive force ratio (N'/N_b', N': axial force, N_b': equilibrium axial force) and ductility ratio for specimens IV-1, VII-1, and VII-2, which had different axial compressive stresses. This figure tells us that the ductility ratio of RC columns retrofitted with our method gradually decrease as the axial compressive stress rises. This tendency matches that of normal reinforced concrete columns [4].

4. CONCLUSIONS

Cyclic loading tests were conducted on retrofitted RC columns in order to check the effectiveness of a new seismic retrofitting method in which external lateral reinforcement is arranged around the column and fixed at the four corners with L-shaped steel anchors. In the specimens tested, the ratio of shear span to effective depth was about 3.0. The following conclusions can be drawn from the experiments and discussions.

a) With the new seismic retrofitting method, the failure mode of RC columns changes from shear to flexural and the ductility of the columns is increased.
b) The ductility of the retrofitted RC columns is not affected much by the post-cast mortar except near the anchorages.
c) Separation of about 20 mm between the external lateral reinforcements and the surface of the existing RC columns has little influence on ductility.
d) Separation of the corner L-shaped steel anchors had little influence on ductility as long as the anchorages remained undamaged.
e) When the axial compressive stress was 0.98 N/mm^2, the ductility ratio of the retrofitted RC columns was over 10 when the shear-to-flexural capacity ratio was above than 1.0. The ductility ratio exceeded 15 for columns whose shear-to-flexural capacity ratio was grater than 1.4.
f) When the axial compressive stress was 0.98 N/mm^2 and the shear-to-flexural capacity ratio was over 1.4, retrofitted RC columns failed by ductile flexural failure.
g) When the axial compressive stress was 5.89 N/mm^2, the ductility of retrofitted RC columns was about 11 when the shear-to-flexural capacity ratio was 1.5. When the axial compressive stress was 9.81 N/mm^2, the ductility dropped to about 8 with shear-to-flexural capacity ratio of 1.5. The higher the axial compressive stress, the lower the ductility. However, in the case of high axial compressive stress, final failure of the retrofitted RC columns was brittle with a sudden drop of load after sufficient deformation.

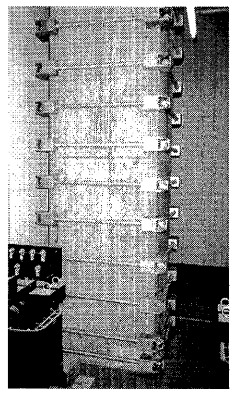

Picture 6 Example of seismic retrofitting of actual RC column

Picture 6 shows an example of seismic retrofitting on an actual RC column. This is thought to be a practical method, especially for use where the space under the superstructure of a viaduct is used by shops or when it is difficult to secure adequate space for other construction methods.

References

[1]Railway Technical Research Institute, Standard specification for design of concrete structure for railways, 1992 (in Japanese)
[2]Mutsuyoshi, H., and Machida, A., "Shear Strength and Ductility of Reinforced Concrete Members Having Longitudinal Reinforcement in Side of Web, Prc. of JCI, No.9-2, pp.335-340, 1987 (in Japanese)
[3]Shima, H., Chou, L., and Okamura, H., "Bond-Slip-Strain Relationship of Deformed Bars Embedded in Massive Concrete", Proc. of JSCE, No.378/V-6, pp.165-174, 1987 (in Japanese)
[4]Railway Technical Research Institute, Standard specification for seismic design of structures for railways, 1999 (in Japanese)